

## Reduction of Electrical Defects in Atomic Layer Deposited HfO<sub>2</sub> Films by Al Doping

Tae Joo Park,<sup>†,‡</sup> Jeong Hwan Kim,<sup>†,‡</sup> Jae Hyuck Jang,<sup>†</sup> Choong-Ki Lee,<sup>§</sup> Kwang Duk Na,<sup>†</sup>  
Sang Young Lee,<sup>†</sup> Hyung-Suk Jung,<sup>†</sup> Miyoung Kim,<sup>†</sup> Seungwu Han,<sup>†</sup> and  
Cheol Seong Hwang<sup>\*,†</sup>

<sup>†</sup>Department of Materials Science and Engineering and Inter-university Semiconductor Research Center, Seoul National University, Seoul 151-744, Korea, and <sup>§</sup>School of Physics, Korea Institute for Advanced Study, Seoul 130-722, Korea. <sup>‡</sup>These authors equally contributed to this work

Received February 28, 2010. Revised Manuscript Received June 9, 2010

The gate leakage current density ( $J_g$ ) of ultrathin ( $\sim 3$  nm) Al-doped HfO<sub>2</sub> (Al:HfO<sub>2</sub>) films with an Al concentration of  $\sim 11\%$  was lower than that of the control HfO<sub>2</sub> film by 2 orders of magnitude at an equivalent oxide thickness of  $\sim 1$  nm. The permittivity of the Al:HfO<sub>2</sub> film was similar to that of the control HfO<sub>2</sub> film. Al doping of HfO<sub>2</sub> films reduced the concentration of the oxygen vacancies and carbon in the film, which act as electrical defects (traps). It also increased the band gap of the film, resulting in a reduced  $J_g$ . Although the crystalline structure of a  $\sim 12$  nm-thick Al:HfO<sub>2</sub> film contained both tetragonal and monoclinic phases after high temperature annealing, the  $\sim 3$  nm thick Al:HfO<sub>2</sub> film showed a monoclinic structure, which is the same as the control HfO<sub>2</sub> film. Therefore, there was no modification of the crystalline structure of the Al:HfO<sub>2</sub> film in the ultrathin film case that would increase the permittivity. However, Si diffusion into the film and interfacial layer growth during annealing were suppressed significantly, which improved the thermal stability of the Al:HfO<sub>2</sub> films.

### Introduction

Recently, post high- $k$  gate dielectric materials with superior properties over that of the conventional high- $k$  materials (HfO<sub>2</sub>, ZrO<sub>2</sub>, etc.) have been studied extensively to be used in advanced gate-stack structures in further-scaled metal-oxide-semiconductor field effect transistors (MOSFETs).<sup>1,2</sup> Most methods for improving the electrical properties of high- $k$  films are based on the incorporation of small concentrations of another material (doping)

into conventional binary oxide high- $k$  films.<sup>3–20</sup> In several experiments reporting the improved properties in doped high- $k$  films, the increased permittivity was mainly attributed to the change in the crystalline structure of the film.<sup>14–20</sup> It was reported that the  $k$  values of HfO<sub>2</sub> and ZrO<sub>2</sub> are enhanced by doping with Y<sub>2</sub>O<sub>3</sub>, Al<sub>2</sub>O<sub>3</sub>, SiO<sub>2</sub>, etc. The crystalline structures of HfO<sub>2</sub> and ZrO<sub>2</sub> were modified by doping from monoclinic to tetragonal or cubic phases, which have a higher permittivity.<sup>21–24</sup> Therefore, a systematic understanding of the improved properties of doped high- $k$  film from the other viewpoints

\*To whom correspondence should be addressed. E-mail: cheolsh@snu.ac.kr.

- (1) Wilk, G. D.; Wallace, R. M.; Anthony, J. M. *J. Appl. Phys.* **2000**, *87*, 484.
- (2) Robertson, J. *Rep. Prog. Phys.* **2006**, *69*, 327.
- (3) Zhang, M. H.; Rhee, S. J.; Kang, C. Y.; Choi, C. H.; Akbar, M. S.; Krishnan, S. A.; Lee, T.; Ok, I. J.; Zhu, F.; Kim, H. S.; Lee, J. C. *Appl. Phys. Lett.* **2005**, *87*, 232901.
- (4) Yan, J.; Kuo, Y.; Lu, J. *Electrochem. Solid-State Lett.* **2007**, *10*, H199.
- (5) Cho, M.-H.; Moon, D. W.; Park, S. A.; Rho, Y. S.; Kim, Y. K.; Jeong, K.; Chang, C. H.; Gu, J. H.; Lee, J. H.; Choi, S. Y. *Appl. Phys. Lett.* **2004**, *84*, 678.
- (6) Lu, J.; Kuo, Y.; Tewg, J.-Y. *J. Electrochem. Soc.* **2006**, *153*, G410.
- (7) Tewg, J.-Y.; Kuo, Y.; Lu, J.; Schueler, B. W. *J. Electrochem. Soc.* **2004**, *151*, F59.
- (8) Kuo, Y.; Lu, J.; Yan, J.; Yuan, T.; Kim, H. C.; Peterson, J.; Gardner, M.; Chatterjee, S.; Luo, W. *ECS Trans.* **2005**, *1*, 447.
- (9) Senzaki, Y.; Park, S.; Chatham, H.; Bartholomew, L.; Nieveen, W. *J. Vac. Sci. Technol., A* **2004**, *22*, 1175.
- (10) Zhu, W. J.; Tamagawa, T.; Gibson, M.; Furukawa, T.; Ma, T. P. *IEEE Electron Device Lett.* **2002**, *23*, 649.
- (11) Rhee, S. J.; Kang, C. S.; Choi, C. H.; Kang, C. Y.; Krishnan, S. A.; Zhang, M. H.; Akbar, M. S.; Lee, J. C. *IEEE Tech. Dig.-Int. Electron Devices Meet.* **2004**, 837.
- (12) Yang, Y.; Zhu, W.; Ma, T. P.; Stemmer, S. *J. Appl. Phys.* **2004**, *95*, 3772.

- (13) Yamamoto, Y.; Kita, K.; Kyuno, K.; Toriumi, A. *Appl. Phys. Lett.* **2006**, *89*, 032903.
- (14) Kita, K.; Kyuno, K.; Toriumi, A. *Appl. Phys. Lett.* **2005**, *86*, 102906.
- (15) Tomida, K.; Kita, K.; Toriumi, A. *Appl. Phys. Lett.* **2006**, *89*, 142902.
- (16) Boscke, T. S.; Govindarajan, S.; Kirch, P. D.; Hung, P. Y.; Krug, C.; Lee, B. H.; Heitmann, J.; Schroder, U.; Pant, G.; Gnade, B. E.; Krautschneider, W. H. *Appl. Phys. Lett.* **2007**, *91*, 072902.
- (17) Triyoso, D. H.; Hegde, R. I.; Schaeffer, J. K.; Roan, D.; Tobin, P. J.; Samavedam, S. B.; White, B. E., Jr.; Gregory, R.; Wang, X.-D. *Appl. Phys. Lett.* **2006**, *88*, 222901.
- (18) Hegde, R. I.; Triyoso, D. H.; Samavedam, S. B.; White, B. E., Jr. *J. Appl. Phys.* **2007**, *101*, 074113.
- (19) Triyoso, D. H.; Hegde, R. I.; Schaeffer, J. K.; Gregory, R.; Wang, X.-D.; Canonico, M.; Roan, D.; Hebert, E. A.; Kim, K.; Jiang, J.; Rai, R.; Kaushik, V.; Samavedam, S. B.; Rochat, N. *Appl. Phys. Lett.* **2006**, *88*, 222901.
- (20) Park, P. K.; Kang, S.-W. *Appl. Phys. Lett.* **2006**, *89*, 192905.
- (21) Zhao, X.; Vanderbilt, D. *Phys. Rev. B.* **2002**, *65*, 233106.
- (22) Lee, C.-K.; Cho, E.; Lee, H.-S.; Hwang, C. S.; Han, S. *Phys. Rev. B.* **2008**, *78*, 012102.
- (23) Fujimori, H.; Yashima, M.; Sasaki, S.; Kakihana, M.; Mori, T.; Tanaka, M.; Yoshimura, M. *Chem. Phys. Lett.* **2001**, *346*, 217.
- (24) Bernay, C.; Ringuede, A.; Colomban, P.; Lincot, D.; Cassir, M. *J. Phys. Chem. Solids.* **2003**, *64*, 1761.

is insufficient. In addition, the improved properties of doped high- $k$  films with an amorphous structure are difficult to explain using the crystalline structure model at present. In addition, the crystallization of high- $k$  films is affected not only by doping but also by other factors, such as the film thickness, stress from the substrate, and the diffusion of substrate elements. Therefore, it is important to examine the parameters that affect the crystalline structure of doped high- $k$  films.

In this study, Al-doped  $\text{HfO}_2$  (Al:HfO<sub>2</sub>) films with various Al concentrations were grown by atomic layer deposition (ALD). The electrical and chemical properties as well as the thermal stability of the films were evaluated. The origins of the improved electrical properties were examined systematically by analyzing the following: (i) the chemical structure, (ii) the state of electrical defects, (iii) the electronic structures, (iv) the crystalline structures, and (v) the interfacial reactions of the Al:HfO<sub>2</sub> films with the Si substrate.

### Experimental Section

**Sample Preparations.** The control HfO<sub>2</sub> and Al-doped HfO<sub>2</sub> thin films were grown to a thickness of  $\sim 3$  to  $\sim 20$  nm at 280 °C on 4 in. diameter p-type (100) Si substrates by thermal ALD using Hf[N(CH<sub>3</sub>)(C<sub>2</sub>H<sub>5</sub>)<sub>3</sub>]<sub>4</sub> (TEMAH) and Al(CH<sub>3</sub>)<sub>3</sub> (TMA) as the Hf and Al precursors, respectively. O<sub>3</sub> at a concentration of 165 g/m<sup>3</sup> was used as the oxygen source. An Al–O layer was inserted discretely into the film by substituting one Hf–O cycle with one Al–O cycle among a total of 30 ALD cycles to allow the incorporation of Al ions into the films. Accordingly, to grow the control HfO<sub>2</sub> and Al-doped HfO<sub>2</sub> films with different Al concentrations, we controlled the number of ALD cycles to 30 (TEMAH) for the control HfO<sub>2</sub> film, 15(TEMAH)/1(TMA)/14 (TEMAH) for the HAO1 film, 10/1/9/1/9 for the HAO2 film, and 7/1/7/1/7/1/6 for the HAO3 film. PDA was performed by rapid thermal annealing at 850 °C for 30 s under a N<sub>2</sub> atmosphere. Sputtered Pt as the top electrode was deposited through a shadow mask to fabricate the metal–insulator–semiconductor capacitors. Forming gas annealing was performed at 400 °C for 10 min in a 95% N<sub>2</sub>/5% H<sub>2</sub> atmosphere after the formation of a Pt top electrode.

**Analyses and Measurements.** The depth profiles of the chemical compositions in the control HfO<sub>2</sub> and Al:HfO<sub>2</sub> films were examined by time-of-flight SIMS. The quantitative chemical compositions of the control HfO<sub>2</sub> and Al:HfO<sub>2</sub> films were estimated by a STEM-EDS and RBS under an oxygen resonance condition (He<sup>+</sup> ion acceleration energy of 3.04 MeV) to observe the oxygen concentration precisely. The chemical binding status and valence band spectra of the film was examined by high resolution XPS using Al K $\alpha$  as the X-ray source. The binding energies of the XP spectra were calibrated using the Si–Si binding energy in the Si 2p XP spectra from the Si substrate (99.0 eV). The thicknesses and microstructures of the films were observed by HRTEM equipped with a field emission electron gun. The physical thicknesses of the films were also measured by ellipsometry. The typical capacitance–voltage ( $C$ – $V$ ) and  $J_g$ – $V$  measurements were performed using an HP 4194 impedance analyzer and HP 4140B picoammeter/dc voltage source, respectively. The EOT was calculated from the accumulation capacitance using the two frequency method<sup>25</sup> considering the quantum mechanical effect. The frequencies of the  $C$ – $V$  measurement were 500 kHz and 1 MHz. The  $V_{\text{FB}}$  value was

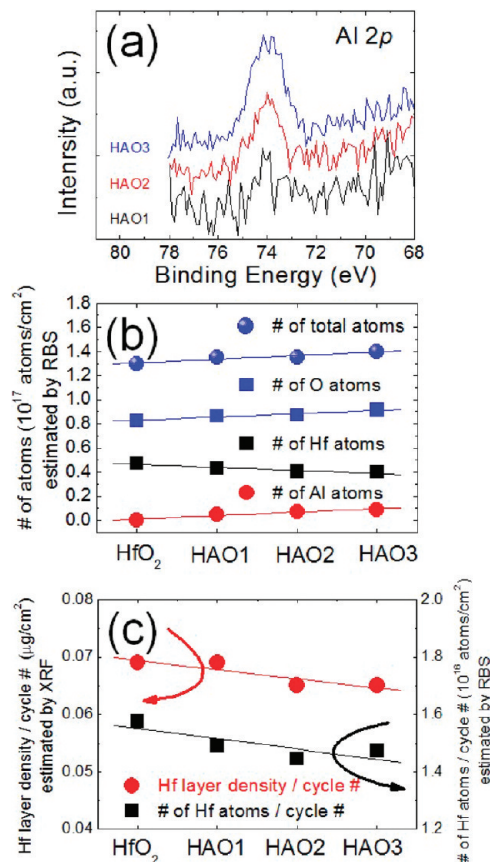


**Figure 1.** (a) Al 2p core level XP spectra of the Al:HfO<sub>2</sub> films, (b) number of O, Hf, Al, and total ions measured by RBS for the control HfO<sub>2</sub> and Al:HfO<sub>2</sub> films, and (c) Hf layer density and number of Hf ions per ALD cycle of Hf–O estimated by XRF and RBS.

determined from the calculated flatband capacitance values using the measured  $C$ – $V$  curve. The size of the top electrodes was measured carefully by optical microscopy. For an analysis of the  $J_g$  mechanism, the  $J_g$ – $V$  characteristics were collected at several different temperatures (from 75 to 135 °C) using an HP 4145B semiconductor parameter analyzer.

**Theoretical Calculations.** Theoretical investigations were performed based on density functional theory. The optimized atomic and electronic structure were examined using a Vienna ab initio simulation package.<sup>26,27</sup> The generalized gradient approximation was used for exchange–correlation potential, and projector-augmented wave method was employed to describe the electron–ion interaction. The k-points were sampled with  $2 \times 2 \times 2$  uniform grids. Plane waves up to an energy cutoff of 500 eV were used to expand the electronic wave functions. The forces on the atoms and stress on the cell were reduced to below 0.02 eV/Å and 1 kb, respectively.

### Results and Discussion

**Chemical and Physical Structures of Al:HfO<sub>2</sub> Thin Films.**  $\sim 3$ – $20$  nm thick Al:HfO<sub>2</sub> films with three different Al concentrations (HAO1, HAO2, and HAO3, where HAO3 has the highest Al concentration) were prepared (see the Experimental Section). The Al 2p core level X-ray photoelectron (XP) spectra of Al:HfO<sub>2</sub> films in Figure 1(a) shows an increase in the Al concentration in the films with

(25) Nara, A.; Yasuda, N.; Satake, H.; Toriumi, A. *IEEE Trans. Semicond. Manuf.* **2002**, *15*, 2.

(26) Kresse, G.; Hafner, J. *Phys. Rev. B* **1993**, *47*, 558(R).

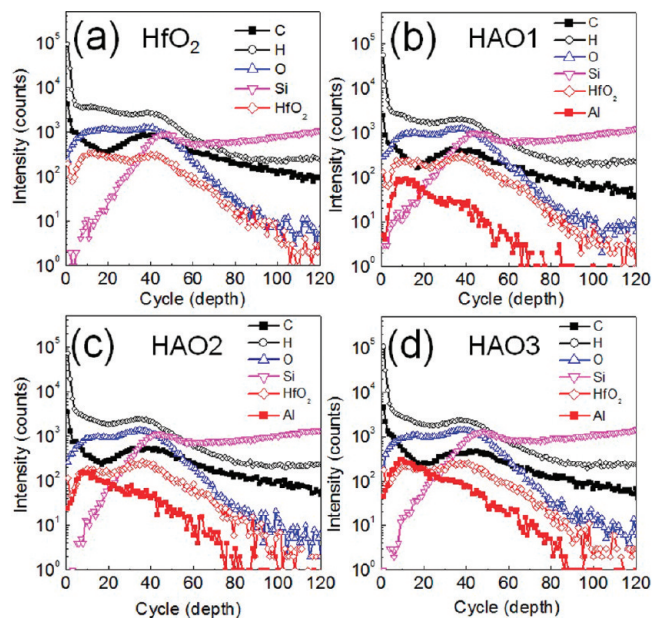
(27) Kresse, G.; Hafner, J. *Phys. Rev. B* **1994**, *49*, 14251.

**Table 1.** Al Concentrations in the Al:HfO<sub>2</sub> Films Estimated by XPS, RBS, STEM EDS, and Calculation Using the Bulk Atomic Density of HfO<sub>2</sub> and Al<sub>2</sub>O<sub>3</sub>

	methods	HAO1	HAO2	HAO3
Al/(Hf + Al) (%)	by RBS (~20 nm)	10.8	15.3	18
	by XPS (~20 nm)	6.5	11.5	17.4
	by STEM EDS (~3 nm)		11.4	
	ideal	5.5	10.8	15.8

increasing ALD cycle number of Al–O. The thickness of the Al:HfO<sub>2</sub> films used for XP spectroscopy (XPS) analysis in Figure 1a was controlled to ~20 nm by repeating the unit 30 ALD cycles to remove the interface effects at the interface with the Si substrate on Al incorporation into the film. Figure 1b shows the atomic number density (number of atoms per volume) of each element in the control HfO<sub>2</sub> and Al:HfO<sub>2</sub> films, which was estimated by Rutherford backscattering spectroscopy (RBS) under the oxygen resonance condition. The film thickness was the same (~20 nm) as those used for XPS analysis in Figure 1a. The atomic density of Hf and Al respectively decreased and increased with increasing number of ALD cycles of Al–O. The growth rates of the ALD HfO<sub>2</sub> and Al<sub>2</sub>O<sub>3</sub> films were similar, ~0.09 nm/cycle. This means that the combined volume of HfO<sub>2</sub> and Al<sub>2</sub>O<sub>3</sub> molecules deposited per ALD cycle is similar. The bulk atomic density of HfO<sub>2</sub> and Al<sub>2</sub>O<sub>3</sub> films was ~0.046 and ~0.039 mol/cm<sup>3</sup>, respectively. Therefore, the amount of Hf and O ions (for HfO<sub>2</sub>) deposited per an ALD cycle of Hf–O is proportional to the bulk atomic density of HfO<sub>2</sub>, ~0.046 and ~0.092 mol/cm<sup>3</sup> (0.046 mol/cm<sup>3</sup> × 2), respectively, because the number of Hf and O ions per a single HfO<sub>2</sub> molecule is one and two, respectively. In the same respect, the amount of Al and O ions (for Al<sub>2</sub>O<sub>3</sub>) deposited per an ALD cycle of Al–O is also proportional to the bulk atomic density of Al<sub>2</sub>O<sub>3</sub>, ~0.078 (≈ 0.039 × 2) and ~0.117 mol/cm<sup>3</sup> (≈ 0.039 × 3), respectively, because the number of Al and O ions per a single Al<sub>2</sub>O<sub>3</sub> molecule is two and three, respectively. As a result, when one Hf–O cycle is substituted with one Al–O cycle, the number of O ions and anions (Hf+Al) increased compared to that of the control HfO<sub>2</sub> film, because Al<sub>2</sub>O<sub>3</sub> generated by one Al–O cycle has more O ions than HfO<sub>2</sub> generated by one Hf–O cycle (3 and 2 O ions for Al<sub>2</sub>O<sub>3</sub> and HfO<sub>2</sub>, respectively). This is supported by the increased number of O and total ions with increasing number of ALD cycles of Al–O, as shown in Figure 1b.

The Al concentrations in the Al:HfO<sub>2</sub> films were examined by XPS, RBS and scanning transmission electron microscopy - energy dispersive X-ray spectroscopy (STEM-EDS), as summarized in Table 1. The values for the “ideal”, which were calculated using the bulk atomic density of HfO<sub>2</sub> and Al<sub>2</sub>O<sub>3</sub>, as mentioned above, were also included. The “ideal” Al concentration in the film corresponds to the case where the incorporation rate of each layer (Al–O and Hf–O) into the film was not influenced by the presence of other layer. Figure 1c shows the Hf layer density and number of Hf ions deposited per ALD cycle of Hf–O estimated by X-ray fluorescence (XRF) and RBS, respectively. Both XRF and RBS results showed that the growth of the HfO<sub>2</sub> layer was retarded further with increasing number of ALD cycles of

**Figure 2.** SIMS depth profiles for the (a) control HfO<sub>2</sub> and (b–d) Al:HfO<sub>2</sub> films.

Al–O. Therefore, the measured Al concentration in the Al:HfO<sub>2</sub> films was slightly larger than the “ideal” values, as shown in Table 1.

Although the film thickness used for STEM-EDS was much smaller (~3 nm) than that of the films used for RBS and XPS analyses (~20 nm), the Al concentration in Al:HfO<sub>2</sub> films estimated by STEM-EDS was similar to those of other analyses. Therefore, the effects of the film thickness or interface on the Al concentration in the Al:HfO<sub>2</sub> films appear to be insignificant. To confirm this, the spatial distribution of Al along the vertical direction in the Al:HfO<sub>2</sub> films with a thickness of ~3 nm was traced by the secondary ion mass spectroscopy (SIMS) depth profiles, as shown in Figure 2b–d for HAO1, HAO2, and HAO3, respectively. It is generally difficult to quantify the SIMS signal due to the matrix effect and inaccurate etching rate of the film during the analysis. Therefore, the relative change in the Al signal with respect to the HfO<sub>2</sub> signal was considered. The Al and HfO<sub>2</sub> signals in the upper layer (UL, 0 to ~30 SIMS cycle (depth)) showed similar trends in all Al:HfO<sub>2</sub> films. Both HfO<sub>2</sub> and Al signals increased between SIMS cycle (depth) 0 through 10 and decreased between SIMS cycle (depth) ~10 and ~30 in all Al:HfO<sub>2</sub> films. This suggests that the Al concentration was almost constant along the thickness direction in the UL of Al:HfO<sub>2</sub> films. However, the metal-silicate phase constituting the interfacial layer (IL, ~30 to ~50 SIMS cycle (depth)) contained a smaller Al signal than that in the UL. This is because Hf-silicate formation is more likely than Al-silicate formation in the IL.

The signals of C and H impurities in the Al:HfO<sub>2</sub> films were much lower than those of the control HfO<sub>2</sub> film in the SIM spectra in Figure 2. This became obvious when they were compared with the O signal, which is almost independent of Al doping. In particular, the C concentration in the films was decreased significantly by Al doping. Although the

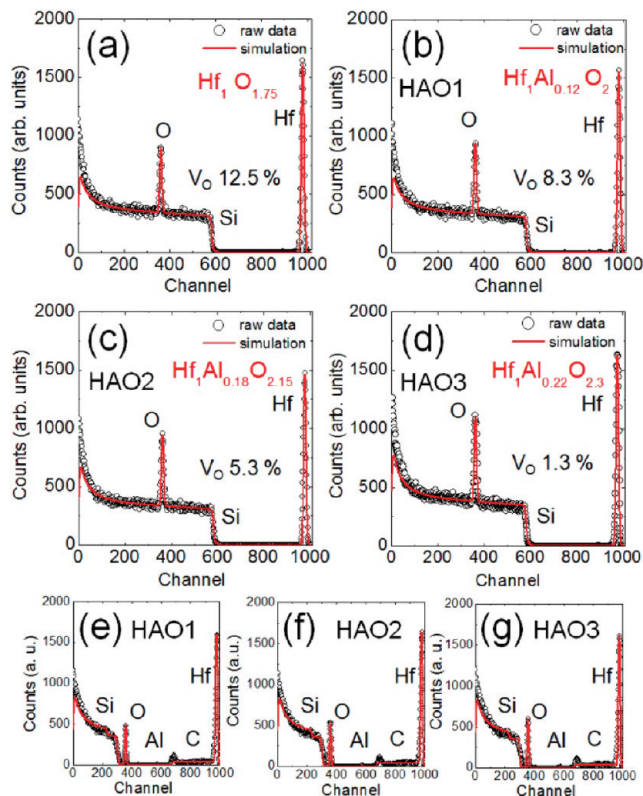


**Figure 3.** RBS results with the oxygen resonance condition for (a) control  $\text{HfO}_2$  and (b–d)  $\text{Al:HfO}_2$  films on Si substrates and (e–g) diamond substrates.

origin of the reduced impurities in the  $\text{Al:HfO}_2$  films is unclear,<sup>28</sup> this appears to have a close relationship with the concentration of oxygen vacancies ( $V_{\text{O}}$ ) in the  $\text{Al:HfO}_2$  films. When a molecule of TEMAH and TMA precursor contains twelve and three C atoms, respectively, it is also possible that the reduced supply of C atoms from the precursor ligands decreased the C concentration in the  $\text{Al:HfO}_2$  films. However, the difference in C concentration between the control  $\text{HfO}_2$  and the  $\text{Al:HfO}_2$  films is much larger than what is expected based on the difference in the supplied amount of C atoms from the precursor ligands. Although the difference in the supplied amount of C atoms between the control  $\text{HfO}_2$  and the  $\text{Al:HfO}_2$  films [TEMAH/TMA ratios of 29/1 (HAO1), 28/2 (HAO2), and 27/3 (HAO3)] is  $\sim 2.5$ – $7.5\%$ , SIMS results showed that the difference in C concentration between the control  $\text{HfO}_2$  and the  $\text{Al:HfO}_2$  films is much larger.

The  $V_{\text{O}}$  concentration in the  $\text{Al:HfO}_2$  films was estimated from the RBS results. Figure 3a–d shows the RBS spectra under the oxygen resonance condition for the control  $\text{HfO}_2$  and  $\text{Al:HfO}_2$  films with a thickness of  $\sim 20$  nm on Si substrates, as mentioned above. Figure 3e–g show the RBS results for the  $\text{Al:HfO}_2$  films on chemical vapor deposited diamond/Si substrates. This substrate provides information (concentrations) of Al in the  $\text{Al:HfO}_2$  films without any interference of the overlapped Si signal from the substrate. The Al concentrations are also summarized in Table 1. The

$V_{\text{O}}$  concentration of  $\sim 12.5\%$  for the control  $\text{HfO}_2$  film decreased to  $\sim 8.3$ ,  $\sim 5.3$ , and  $\sim 1.3\%$  with increasing Al concentration in the  $\text{Al:HfO}_2$  films. Here, the  $V_{\text{O}}$  concentration was determined by comparing the measured O stoichiometry and the ideal stoichiometric value calculated from the measured cation stoichiometry. For example, the stoichiometric HAO2 film ( $\text{Hf:Al} = 1:0.18$ , see Figure 3c), requires 2.27 O atoms per molecule ( $2\text{O}$  for  $1\text{Hf} + 0.27\text{O} (= 0.18 \times 3/2)$  for  $0.18\text{Al}$ ). Considering the measured O stoichiometry is 2.15, the  $V_{\text{O}}$  concentration of the HAO2 is  $\sim 5.3\%$ .  $[(2.27 - 2.15)/2.27] \times 100$  This is not because of the simple replacement of oxygen-deficient  $\text{HfO}_{1.75}$  with stoichiometric  $\text{Al}_2\text{O}_3$ . If this were the case, the oxygen stoichiometry of HAO1, HAO2, and HAO3 would be 1.93 ( $= 1.75 + (0.12 - 3/2) = 1.93$ ), 2.02 ( $= 1.75 + (0.18(3/2)) = 2.02$ ), and 2.08 ( $= 1.75 + (0.22(3/2)) = 2.08$ ), respectively, which is lower than the estimated values of 2.00, 2.15, and 2.30, respectively. This suggests that the  $V_{\text{O}}$  concentration in the  $\text{HfO}_2$  material is decreased by Al doping. This is consistent with the first-principles calculations by X. F. Wang et al., who reported that the presence of Al in  $\text{HfO}_2$  led to the passivation of defect states induced by  $V_{\text{O}}$  in the film.<sup>29</sup> N. Umezawa et al. also reported that that doping materials, such as Ba and La, reduced the  $V_{\text{O}}$  concentrations in  $\text{HfO}_2$  films considerably.<sup>30,31</sup> These changes in the  $V_{\text{O}}$  concentration in the film as a function of the Al concentration are consistent with the electrical defect status estimated by the electrical measurements, which will be discussed in detail later.

The low concentrations of C and H in the  $\text{Al:HfO}_2$  films are closely related to the low  $V_{\text{O}}$  concentration. Dutta et al. recently reported, based on first-principles calculations, that the  $\text{ZrO}_2$  film with  $V_{\text{O}}$  is more stable when there is a similar level of substitution or interstitial C atoms in the film.<sup>32</sup> Suzuki et al. also reported that the reduction of  $V_{\text{O}}$  (addition of more oxygen) in the  $\text{HfO}_2$  eliminated the C-related defect states in the band gap.<sup>33</sup> Therefore, the lower  $V_{\text{O}}$  concentration in the  $\text{Al:HfO}_2$  films could reduce the concentrations of C and H in the films. It is also likely that the high reactivity of the Al precursor [TMA,  $\text{Al}(\text{CH}_3)_3$ ] removed the residual C and H impurities in the film more efficiently.<sup>34</sup> J. Kwon et al. also reported that TMA pulse decreased the residual surface ligands, resulting in the reduction of C impurity in the film.<sup>35</sup>

The microstructures of the as-deposited control  $\text{HfO}_2$  with 30 and 33 ALD cycles, and  $\text{Al:HfO}_2$  film (HAO2) with 30 ALD cycles were observed by cross-sectional high resolution transmission electron microscopy (HRTEM), as shown in

(28) Park, T. J.; Sivasubramani, P.; Coss, B. E.; Lee, B.; Wallace, R. M.; Kim, J.; Liu, X.; Yi, J.; Rousseau, M.; Shenai, D.; Suydam, J. **2010**, unpublished.

(29) Wang, X. F.; Lia, Q.; Egerton, R. F.; Lee, P. F.; Dai, J. Y.; Hou, Z. F.; Gong, X. G. *J. Appl. Phys.* **2007**, *101*, 013514.  
 (30) Umezawa, N. *Appl. Phys. Lett.* **2009**, *94*, 022903.  
 (31) Umezawa, N.; Shiraiishi, K.; Sugino, S.; Tachibana, A.; Ohmori, K.; Kakushima, K.; Iwai, H.; Chikyow, T.; Ohno, T.; Nara, Y.; Yamada, K. *Appl. Phys. Lett.* **2007**, *91*, 132904.  
 (32) Dutta, G.; Hembram, K. P. S. S.; Rao, G. M.; Waghmare, U. V. *Appl. Phys. Lett.* **2006**, *89*, 202904.  
 (33) Suzuki, K.; Ito, Y.; Miura, H. *Proceedings of the 2006 International Conference on Simulation of Semiconductor Processes and Devices*; Monterey, CA, Sept 6–8, 2006; IEEE: Piscataway, NJ, 2007; Vol. 12, p 165.  
 (34) Hinkle, C. L.; Sonnet, A. M.; Vogel, E. M.; McDonnell, S.; Hughes, G. J.; Milojevic, M.; Lee, B.; Aguirre-Tostado, F. S.; Choi, K. J.; Kim, H. C.; Kim, J.; Wallace, R. M. *Appl. Phys. Lett.* **2008**, *92*, 071901.  
 (35) Kwon, J.; Dai, M.; Halls, M. D.; Langereis, E.; Chabal, Y.; Gordon, R. G. *J. Phys. Chem. C* **2009**, *113*, 654.

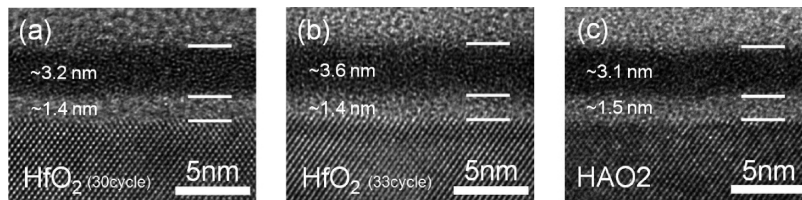


**Figure 4.** Cross-sectional HRTEM images of the as-deposited control  $\text{HfO}_2$  with 30 and 33 ALD cycles, and Al: $\text{HfO}_2$  film (HAO2) with 30 ALD cycles.

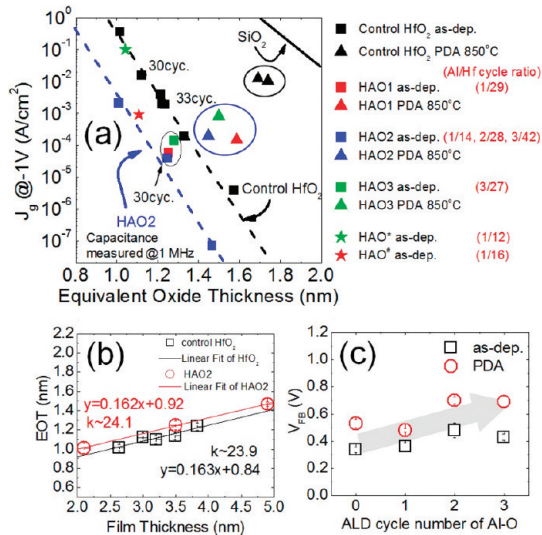


**Figure 5.** (a) Plot of EOT vs  $J_g$  for control  $\text{HfO}_2$  and Al: $\text{HfO}_2$  films (HAO1, HAO2, and HAO3); (b) EOT as a function of physical film thickness for control  $\text{HfO}_2$  and Al: $\text{HfO}_2$  film (HAO2); and (c)  $V_{FB}$  variations for the control  $\text{HfO}_2$  and Al: $\text{HfO}_2$  films.

Figure 4. All the films had amorphous structures. The thickness of each layer is the average value calculated from more than 15 HRTEM images taken from different regions of the film. The UL and IL thicknesses of the control  $\text{HfO}_2$  film with 30 ALD cycles was  $\sim 3.2$  and  $\sim 1.4$  nm, respectively. When the number of ALD cycles was increased to 33, the UL thickness of the control  $\text{HfO}_2$  film increased to  $\sim 3.6$  nm with no notable increase in the IL thickness. The UL and IL thickness of the Al: $\text{HfO}_2$  (HAO2) film was  $\sim 3.1$  and  $\sim 1.5$  nm, respectively. Since the silicate reaction is suppressed during ALD because of the  $\text{Al}_2\text{O}_3$  phase, the UL of the HAO2 film ( $\sim 3.1$  nm) is slightly thinner than that of the control  $\text{HfO}_2$  film ( $\sim 3.2$  nm) with the same (30) ALD cycles. Although HAO2 film was physically thinner than the control  $\text{HfO}_2$  film produced from 33 ALD cycles, the equivalent oxide thickness (EOT) of HAO2 was similar to that of the control  $\text{HfO}_2$  film. This is because the HAO2 film has a thicker IL than the control  $\text{HfO}_2$  film. The electrical properties of the films are discussed in detail below.

**Electrical Properties of the Al: $\text{HfO}_2$  Thin Films.** Figure 5a shows a plot of the EOT versus the gate leakage current density ( $J_g$ ) for the control  $\text{HfO}_2$ , and Al: $\text{HfO}_2$  films (HAO1, HAO2, and HAO3). The black squares indicate the results for the as-deposited control  $\text{HfO}_2$  films with different thicknesses, which are aligned on the black dashed line. The appropriate Al concentrations ( $\sim 10.8\%$  of HAO2 based on the ‘ideal’ value, blue squares and a blue dashed line) in the films reduced the  $J_g$  value by 2 orders of magnitude compared to the control  $\text{HfO}_2$  films. The three HAO2 films

on the blue dashed line were produced from 1/14, 2/28, and 3/42 Al–O/Hf–O ALD cycles (with the same Al–O/Hf–O ALD cycle ratio of 1/14), respectively. The red and green squares indicate the result for the as-deposited HAO1 and HAO3 films (Al concentrations of  $\sim 5.5$  and  $\sim 15.8\%$ ), respectively, of which the dielectric properties were slightly better than those of the control  $\text{HfO}_2$  films but worse than those of the HAO2 films. The red stars and green star indicate the result for the film grown with 1/12 and 1/16 Al/Hf cycles, respectively. These films have a slightly higher and lower Al concentration in the film (Al concentrations of  $\sim 12.5$  and  $\sim 9.5\%$ ), respectively, than the HAO2 film. These Al concentrations in the film degraded the dielectric properties of the films compared to the HAO2 film. Therefore, the dielectric properties of the Al: $\text{HfO}_2$  films improved with increasing Al concentration in the film until a certain optimal point ( $\sim 10.8\%$  in this study, the HAO2 film has the optimized Al concentration for the best electrical properties), then became rapidly worse beyond that optimization point. In Figure 5a the flat band ( $V_{FB}$ ) shift by the different Al-doping concentrations was not considered. When this was considered (i.e.,  $J_g$  at  $V_{FB} - 1$  V), the HAO2 films showed an even better dielectric performance than that shown in Figure 5a.

The permittivity of the films can be calculated using the inverse slope of the EOT vs physical thickness plot, as shown in Figure 5b. Even though the film thickness range may not be wide enough to achieve the permittivity accurately, the thickness range should be limited to the ultrathin region because the main purpose of this study is to examine the film properties in the ultrathin region. Thicker films might be crystallized during ALD, which could induce changes in the permittivity. Interestingly, the permittivity of the HAO2 film ( $\sim 24$ ) was similar to that of the control  $\text{HfO}_2$  film in this thickness region. However, it is expected that the lower permittivity of  $\text{Al}_2\text{O}_3$  began to decrease the permittivity of the Al: $\text{HfO}_2$  film beyond a certain optimization point ( $\sim 10.8\%$  in this study).<sup>36,37</sup> The permittivity of the IL in the control  $\text{HfO}_2$  and HAO2 is also similar, being  $\sim 6.5$  and  $\sim 6.4$ , respectively. (EOT and thickness of the IL provides the information needed to extract the permittivity of the IL). Therefore, the superior electrical properties of Al: $\text{HfO}_2$  films to that of  $\text{HfO}_2$  were due to the reduced  $J_g$  not the enhanced permittivity of the films. S. Jeon et al. reported that ultrathin lanthanide-doped  $\text{HfO}_2$  films grown by e-beam evaporation showed a reduced  $J_g$  without any significant changes in permittivity.<sup>37</sup>

- (36) Govindarajan, S.; Boscke, T. S.; Sivasubramani, P.; Kirch, P. D.; Lee, B. H.; Tseng, H.-H.; Jammy, R.; Schroder, U.; Ramanathan, S.; Gnade, B. E. *Appl. Phys. Lett.* **2007**, *91*, 062906.  
 (37) Jeon, S.; Im, K.; Yang, H.; Lee, H.; Sim, H.; Choi, S.; Jang, T.; Hwang, H. *IEEE Tech. Dig.-Int. Electron Devices Meet.* **2001**, 20(6), 1.

The reduced  $J_g$  of the Al:HfO<sub>2</sub> films is believed to originate from the lower concentrations of V<sub>O</sub> and impurities, such as C and H in the films, as discussed above, which were verified by the electrical measurements and analysis in next section. Although the concentrations of V<sub>O</sub> and impurities in the film were reduced further, the HAO3 film showed degraded properties compared to the HAO2 film. This might be because the decrease in the permittivity of the Al:HfO<sub>2</sub> film by Al<sub>2</sub>O<sub>3</sub> ( $k \approx 8$ ) in the film dominated the advantages from the lower concentrations of V<sub>O</sub> and impurities in the film.<sup>36,37</sup>

The smaller EOT of the control HfO<sub>2</sub> film than that of the HAO2 film with the same thickness (30 cycle,  $\sim 4.6$  nm) was induced by the thicker IL of the HAO2 film, as shown in Figure 4. This is also supported by the results in Figure 5b, which show that the electrical thickness of the IL ( $y$ -intercept) of HAO2 film ( $\sim 0.92$  nm) is larger than that of the control HfO<sub>2</sub> film ( $\sim 0.84$  nm). The reason for the slightly thicker IL in the Al:HfO<sub>2</sub> film is unclear.

The  $V_{FB}$  increased with increasing Al concentration in the Al:HfO<sub>2</sub> film before and after PDA, as shown in Figure 5c, because the Al ions in the HfO<sub>2</sub> films act as the negative fixed charges.<sup>38,39</sup> This provides advantages for a lower  $J_g$  at a lower threshold voltage in the operation of p-MOSFET devices. The annealed Al:HfO<sub>2</sub> films also have superior dielectric properties than the annealed control HfO<sub>2</sub> films. There was not only a decrease in  $J_g$  of approximately 2 orders of magnitude but also an  $\sim 0.3$  nm decrease in the EOT in the case of the HAO2 film. The electrical properties of the annealed Al:HfO<sub>2</sub> films will be discussed later in terms of the chemical and crystalline structures.

**Electronic Band Structure and Defects of Al:HfO<sub>2</sub> Thin Films.** The temperature dependent  $J_g-V$  characteristics of the control HfO<sub>2</sub> and HAO2 films were examined to confirm the effects of the reduced V<sub>O</sub> and impurities by Al-doping on the energy band structure and electrical defects state of the Al:HfO<sub>2</sub> films. The control HfO<sub>2</sub> film with 33 ALD cycles and the HAO2 film with 30 ALD cycles were compared because the two films have a similar EOT, as discussed above. Panels a and b in Figure 6 show the typical  $J_g-V$  curves of the control HfO<sub>2</sub> and the HAO2 films measured at various temperatures ranging from 75 to 135 °C with a negative bias applied to the Pt gate. For a detailed analysis of the conduction mechanism, it is important to know the electric field distribution across the dielectric layer (UL and IL). The electric field across the dielectric film was calculated on the basis of the following formula

$$E = \frac{V_g - V_{FB} - \phi_s}{t} \quad (1)$$

where  $t$  is the physical thickness of the dielectric film, and  $\phi_s$  indicates silicon band-bending. The electric field distribution across the dielectric layer (UL and IL) was considered with

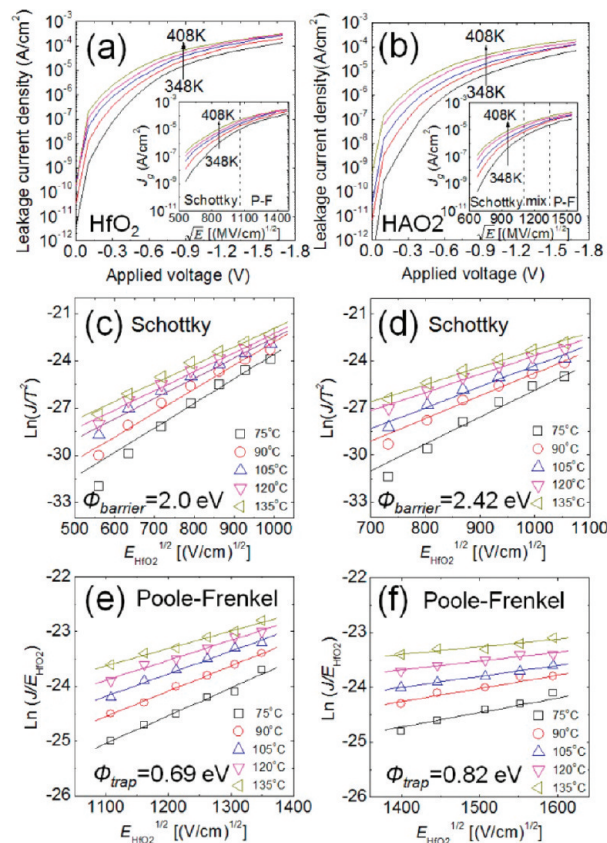


**Figure 6.** (a, b) Typical  $J_g-V$  and  $J_g-E$  curves measured at various temperatures ranging from 75 to 135 °C, respectively. (c, d) electric-field-dependent Schottky emission plots and (e, f) Poole-Frenkel emission plots for the control HfO<sub>2</sub> and Al:HfO<sub>2</sub> (HAO2) films, respectively.

the dielectric constants and physical thicknesses of each layer. The dielectric constants of the UL for both of the control HfO<sub>2</sub> and HAO2 film used to calculate the electric field distribution were 24, which were calculated from the slope of the graph in Figure 5b. The dielectric constants of the IL were assumed to be 6.5 considering the physical thicknesses of the ILs (see Figure 4) and their electrical thickness (see Figure 5b), which is consistent with the values reported elsewhere.<sup>40</sup> The IL thickness of  $\sim 1.4-1.5$  nm for the control HfO<sub>2</sub> and HAO2 film are so thin that it must show direct tunneling behavior of electrons, of which the leakage current should be much higher than the observed leakage current through the entire film. Therefore, the leakage current through the entire film would be determined by the UL, so that electric field of the UL was taken to fit the electric field dependent  $J_g$  in the subsequent analyses of the conduction mechanism.

The appropriate electrical conduction mechanisms of the films were dependent on the electric field region, as shown in the insets in panels a and b in Figure 6. The applied electric field of the control HfO<sub>2</sub> and HAO2 film could be divided into two regions corresponding to Schottky and Poole-Frenkel emission (conduction) regions. There was a third region with mixed conduction behavior of the HAO2 film. In the graph of  $\ln(J_g/T^2)$  vs  $E^{1/2}$  for the control HfO<sub>2</sub> and HAO2 films (Figure 6c, d), the well-fitted straight lines could be

(38) Johnson, R. S.; Lucovsky, G.; Baumvol, I. J. *Vac. Sci. Technol., A* **2001**, *19*, 1353.

(39) Crivelli, B.; Alessandri, M.; Alberici, S.; Cazzaniga, F.; Pavia, G.; Queirolo, G.; Zanderigo, F.; Dekadjevi, D.; Maes, J. W.; Ottaviani, G.; Santucci, S. In *Novel Materials and Processes for Advanced CMOS*; Proceedings of the 2002 Materials Research Society Fall Meeting; Materials Research Society: Warrendale, PA, 2002; Vol. 745, N5.3

(40) Park, P. K.; Roh, J.; Choi, B. H.; Kang, S. *Electrochem. Solid-State Lett.* **2006**, *9*, F34.

obtained in the low-field regions from  $\sim 0.31$  to  $\sim 0.98$  MV/cm, which corresponds to the applied voltage from approximately  $-0.1$  to approximately  $-0.7$  V for the control HfO<sub>2</sub> film, and from  $\sim 0.45$  to  $\sim 1.11$  MV/cm, which corresponds to the applied voltage from approximately  $-0.1$  to approximately  $-0.7$  V for the HAO2 films. In these  $E$  regions, Schottky emission was found to be the dominant conduction mechanism. Schottky emission can be described as follows

$$J = A^*T^2 \exp\left[\frac{-q(\phi_B - \sqrt{qE/4\epsilon\pi})}{kT}\right] \quad (2)$$

where  $A^*$  is the effective Richardson constant, and  $\epsilon$  and  $k$  are the dynamic dielectric constant and the Boltzmann constant, respectively. The  $\epsilon$  value obtained from a fit of Schottky emission ranged from  $\sim 4.03$  and  $\sim 4.82$ , which is similar to the theoretical value ( $n^2 \approx 4.0$ ,  $n$  is the refractive index). The zero-field Schottky barrier height ( $\phi_B$ ) extracted by extrapolating the plot of  $E^{1/2}$  vs  $\phi_B$  under each specific electric field to the zero electric field from the temperature-dependent Schottky emission fitting in panels a and b in Figure 7 was  $\sim 2.00$  and  $\sim 2.42$  eV for the control HfO<sub>2</sub> and HAO2 film, respectively, as shown in panels e and f in Figure 7. Therefore, Al doping in a HfO<sub>2</sub> film increased the  $\phi_B$  by  $\sim 0.42$  eV, which is one of the main causes for the decrease in  $J_g$  of the Al:HfO<sub>2</sub> films.

On the other hand, Poole–Frenkel emission was the dominant conduction mechanism in the high field region from  $\sim 1.22$  to  $\sim 2.22$  MV/cm for the control HfO<sub>2</sub> film, which corresponds to the applied voltage from approximately  $-0.9$  to approximately  $-1.7$  V, and from  $\sim 1.95$  to  $\sim 2.54$  MV/cm for the HAO2 film, which corresponds to the applied voltage from approximately  $-1.4$  to approximately  $-1.8$  V. The  $\ln(J_g/E)$  vs  $E^{1/2}$  plots (Poole–Frenkel plots) showed straight lines, as shown in panels e and f in Figure 6 for the control HfO<sub>2</sub> and HAO2 film, respectively. P–F conduction can be described as follows

$$J = CE \exp\left[\frac{-q(\phi_t - \sqrt{qE/\epsilon\pi})}{kT}\right] \quad (3)$$

The obtained dynamic dielectric constants were reasonable (3.80–4.61). Poole–Frenkel conduction is controlled by the trapping and activation of trapped carriers from bulk traps. The trap energy depth ( $\phi_t$ ) under each specific electric field can be obtained from the slope of the  $\ln(J_g/E)$  vs  $1/T$  plot in panels c and d in Figure 7. Therefore, the intrinsic  $\phi_t$  value without the field effect can be extracted by extrapolating the curve to zero electric field, as shown in panels g and h in Figure 7. The extracted  $\phi_t$  value for the control HfO<sub>2</sub> and HAO2 film was  $\sim 0.69$  and  $\sim 0.82$  eV, respectively.<sup>41</sup> It was reported that V<sub>O</sub> in the HfO<sub>2</sub> film produced shallow trap level of  $\sim 0.5$  eV beneath the conduction band edge.<sup>42</sup> Therefore, the higher estimated  $\phi_t$  value suggests that Al doping removed these shallow defect states. This also contributed to the decrease in  $J_g$  of the Al:HfO<sub>2</sub> films.

In the middle field region from  $\sim 1.11$  to  $\sim 1.95$  MV/cm, which corresponds to the applied voltage from approximately  $-0.7$  to approximately  $-1.4$  V, the HAO2 film

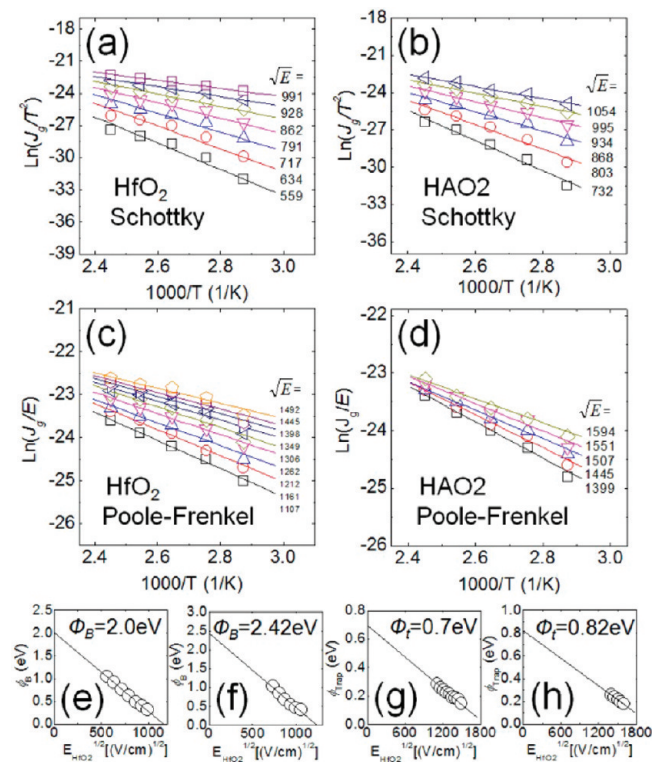


**Figure 7.** (a, b) Temperature-dependent Schottky emission plots, (c, d) Poole–Frenkel emission plots, (e, f) Schottky barrier height ( $\phi_B$ ) under each specific electric field from the temperature-dependent Schottky plot, (g, h) trap energy depth ( $\phi_t$ ) under each specific electric field from the temperature-dependent Poole–Frenkel plot for the control HfO<sub>2</sub> and Al:HfO<sub>2</sub> (HAO2) films, respectively.

showed a mixed conduction mechanism, as indicated in the inset figure of Figure 6b, where the conduction behavior is difficult to be defined by only one mechanism; either Schottky or Poole–Frenkel emission.

With increasing electric field over the UL, the electrons transport to the traps through a more tunneling-like mechanism rather than by thermionic emission. Therefore, with increasing voltage, the films show a transition from Schottky emission to Poole–Frenkel behavior.

Even though the lower  $J_g$  of HAO2 in the Poole–Frenkel conduction region can be explained by its lower trap concentration, the  $J_g$  in the Schottky region, where the plot of EOT– $J_g$  measured at  $-1$  V in Figure 5 was taken, is mostly dominated by the band structure (band offset) of the film. Therefore, the energy band structures of the Pt-gated control HfO<sub>2</sub> and HAO2 film on Si were examined by XPS, and the electrical measurement results. The band gap energy of the control HfO<sub>2</sub> and HAO2 films was estimated from the O 1s loss spectra, as shown in Figure 8a. The band gap energy of the film was determined by the energy separation between the peak energy and threshold energy of the loss spectrum because a photoelectron loses its kinetic energy by a Plasmon and band to band excitation.<sup>43</sup> The estimated band gap energy of the control HfO<sub>2</sub> and HAO2 films was  $\sim 5.05$  and  $\sim 5.40$  eV, respectively. The XPS valence band spectra provide information on the energy distance between the Fermi energy level ( $E_F$ ) and upper edges of the valence band

(41) Yeh, C.-C.; Ma, T. P.; Ramaswamy, N.; Rocklein, N.; Gealy, D.; Graettinger, T.; Min, K. *Appl. Phys. Lett.* **2007**, *91*, 113521.

(42) Xiong, K.; Robertson, J.; Clark, S. J. *J. Appl. Phys.* **2006**, *99*, 044105.

(43) Miyazaki, S. *Appl. Surf. Sci.* **2002**, *190*, 66.

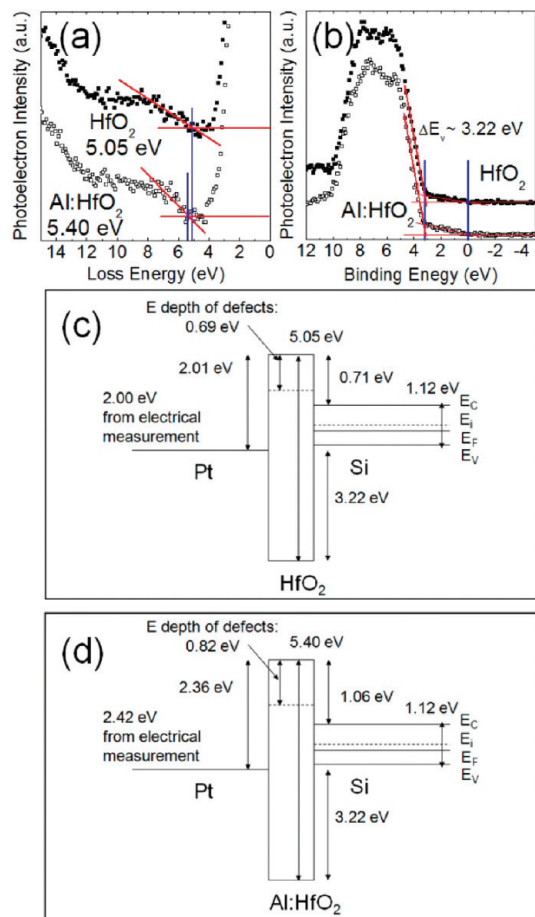


**Figure 8.** (a) O 1s loss spectra, (b) valence band spectra, and (c, d) reconstructed band structures based on the XPS results and electrical measurements of the control HfO<sub>2</sub> and Al:HfO<sub>2</sub> (HAO2) film on Si, respectively.

( $E_V$ ) of the films and Si substrate. Therefore, the valence band offset with a Si substrate can be obtained from the XPS valence band spectra, as shown in Figure 8b. The estimated valence band offset with a Si substrate of both films was the same,  $\sim 3.22$  eV. Similar results were reported by M. Komatsu et al., where the valence band offset of HfO<sub>2</sub>/Si was almost unchanged by Y-doping.<sup>44</sup> The band gap energy of Si is  $\sim 1.12$  eV. The work function of Pt was  $\sim 5.25$  eV,<sup>45</sup> which was obtained experimentally from y-intercept value in the  $V_{FB}$  vs EOT plot of the films with various thickness (data not shown). As a result, the band structures of the Pt-gated control HfO<sub>2</sub> and Al:HfO<sub>2</sub> films on a Si substrate could be reconstructed, as shown in panels c and d in Figure 8. The  $\phi_B$  values between Pt and the films ( $\sim 2.01$  and  $\sim 2.36$  eV for the control HfO<sub>2</sub> and Al:HfO<sub>2</sub> film, respectively) in the reconstructed band structures are consistent with the  $\phi_B$  values ( $\sim 2.00$  and  $\sim 2.42$  eV for the control HfO<sub>2</sub> and Al:HfO<sub>2</sub> film, respectively) estimated from the Schottky emission fitting shown in Figure 6. The larger  $\phi_B$  for the HAO2 films in the Schottky emission simulation originated from the increased band-gap energy.

Panels a and b in Figure 9 show the density of states (DOS) for the control HfO<sub>2</sub> and Al:HfO<sub>2</sub> films (Al concentration of  $\sim 3$  atomic %), respectively, extracted by first-principles calculations based on density functional methods. Here, V<sub>O</sub> and C impurities were not considered. The top of the valence band was set to zero in all cases. Although the materials have an amorphous structure, a crystalline structure must be assumed for first principle calculations because a regular atomic structure of the material is needed. Therefore, the crystalline structures of the films were assumed to be a monoclinic phase, which is closest to the amorphous phase. A supercell containing 96 atoms was used and an Al atom was substituted for the Hf site. The supercell was obtained by doubling the unitcell of monoclinic HfO<sub>2</sub> along each axis. The calculated band gap energies of the control HfO<sub>2</sub> and Al:HfO<sub>2</sub> film were similar ( $\sim 4.0$  eV). Considering the well-known underestimation of the band gap in the density functional method, this suggests that Al<sub>2</sub>O<sub>3</sub> itself in Al:HfO<sub>2</sub> film is not the main cause of the increased band-gap energy of the Al:HfO<sub>2</sub> film.

X. F. Wang et al. also reported that Al in the HfO<sub>2</sub> had little effect on the band gap energy of HfO<sub>2</sub>.<sup>29</sup> G. Dutta et al. recently reported a first-principles study of the effect of V<sub>O</sub> and C doping on the dielectric properties of ZrO<sub>2</sub>. They showed that the band gap energy of a ZrO<sub>2</sub> film was increased by the reduction of V<sub>O</sub> and C impurities in the film.<sup>32</sup> Suzuki et al. also reported that stoichiometric HfO<sub>2</sub> has a larger band gap energy than HfO<sub>2</sub> with C impurities.<sup>33</sup> Therefore, the band gap energy of the Al:HfO<sub>2</sub> film may have increased as the concentration of V<sub>O</sub> and C is reduced. Although the band gap energies of the thin ILs are hard to determine, it is believed that they are similar in both films because the ILs are mostly composed of SiO<sub>2</sub> and have similar dielectric constants as mentioned above.

**Thermal Stability of Al:HfO<sub>2</sub> Thin Films.** PDA at a high temperatures generally degrades the dielectric properties of the high- $k$  gate dielectric films because Si diffuses from the substrate into the films (Hf-silicate reaction) and oxidation of the Si substrate at the interface with the film (IL growth) during PDA increases the EOT of the film. In addition, the degraded interfacial properties and crystallization of the film by PDA at a high temperature increases the  $J_g$  of the film.<sup>46–49</sup> These adverse interfacial and structural effects eventually degrade the MOSFET performance. Therefore, the dielectric properties of both the control HfO<sub>2</sub> and Al:HfO<sub>2</sub> film were degraded after PDA at 850 °C, as shown in Figure 5a. Although  $J_g$  increased by an order of magnitude for both the control HfO<sub>2</sub> and Al:HfO<sub>2</sub> films, the differences in  $J_g$  ( $\sim 2$  orders of magnitude for HAO2) was maintained even after PDA. The increase in the EOT after PDA was also suppressed in

- (44) Komatsu, M.; Yasuhara, R.; Takahashi, H.; Toyoda, S.; Kumigashira, H.; Oshimaa, M.; Kukuruzyak, D.; Chikyow, T. *Appl. Phys. Lett.* **2006**, *89*, 172107.  
 (45) Todi, R. M.; Erickson, M. S.; Sundaram, K. B.; Barmak, K.; Coffey, K. R. *IEEE Trans. Electron Devices* **2007**, *54*, 4.

- (46) Park, J.; Cho, M.; Kim, S. K.; Park, T. J.; Lee, S. W.; Hong, S. H.; Hwang, C. S. *Appl. Phys. Lett.* **2005**, *86*, 112907.  
 (47) Park, T. J.; Kim, J. H.; Jang, J. H.; Na, K. D.; Hwang, C. S.; Yoo, J. H. *Electrochem. Solid-State Lett.* **2008**, *11*, H121.  
 (48) Yamaguchi, T.; Iijima, R.; Ino, T.; Nishiyama, A.; Satake, H.; Fukushima, N. *IEEE Tech. Dig.—Int. Electron Devices Meet.* **2001**, 451.  
 (49) Park, T. J.; Kim, J. H.; Jang, J. H.; Seo, M.; Na, K. D.; Hwang, C. S. *Microelectron. Eng.* **2007**, *84*, 2226.

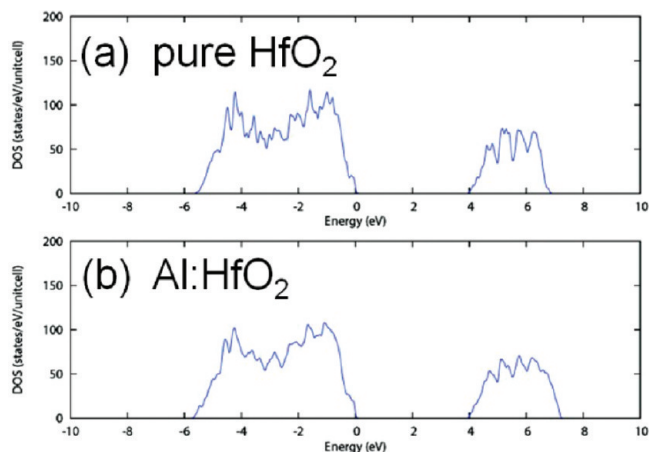


Figure 9. Density of state plots of (a) control HfO<sub>2</sub> and (b) Al:HfO<sub>2</sub> film.

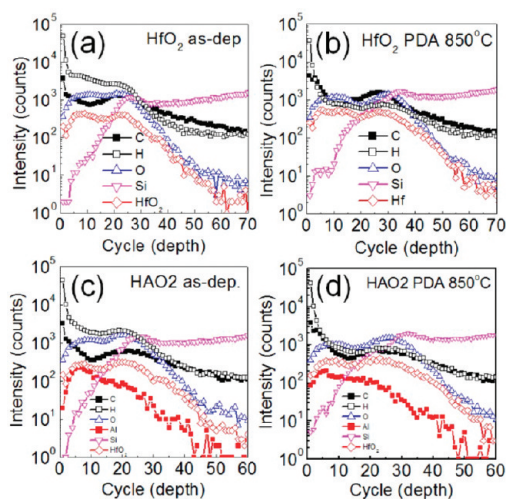


Figure 10. SIMS depth profiles of the control HfO<sub>2</sub> and Al:HfO<sub>2</sub> (HAO2) film (a,c) before and (b,d) after PDA.

case of the Al:HfO<sub>2</sub> films (~0.2 nm) compared to the control HfO<sub>2</sub> film (~0.5 nm) as shown in Figure 5a.

The crystalline and chemical structures of the Al:HfO<sub>2</sub> films were analyzed to explain the improvement in thermal stability of electrical properties against degradation by PDA. The chemical structures of the films were examined by SIMS depth profiling for the control HfO<sub>2</sub> and HAO2 film before and after PDA, as shown in Figure 10. PDA reduced the concentration of H impurity in both films. However, the control HfO<sub>2</sub> and HAO2 film showed similar chemical structural changes after PDA. The change in the Al profile in the film after PDA was also negligible. Considering that the  $J_g$  level of the film was determined mainly by the C and  $V_O$  concentration in the film, the lack of a difference in the chemical structural changes by PDA is consistent with the fact that the differences in  $J_g$  (~2 orders of magnitude for HAO2) between the control HfO<sub>2</sub> and HAO2 film had been preserved, even after PDA.

The EOT increase during the PDA is suppressed by the increased permittivity of the film or the suppressed Hf-silicate reaction and IL growth. It was reported that doped HfO<sub>2</sub> and ZrO<sub>2</sub> films have a tetragonal or cubic phase, which has a larger permittivity ( $\geq 30$ ) than a monoclinic phase

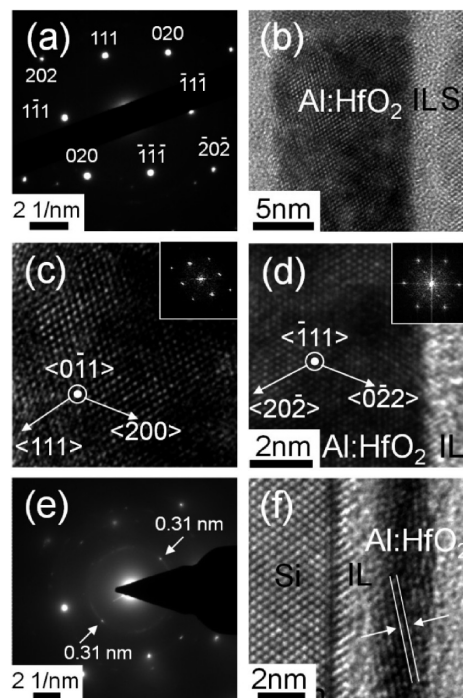
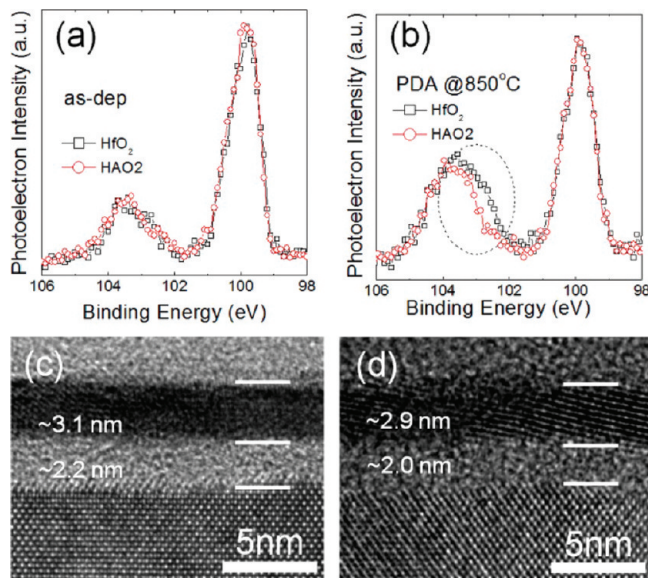


Figure 11. (a) SADP, (b–d) cross-sectional HRTEM images, (insets of c and d) FFT images for ~12 nm-thick Al:HfO<sub>2</sub> (HAO2) film, and (e, f) plan-view DP and cross-sectional HRTEM image of ~3 nm-thick Al:HfO<sub>2</sub> (HAO2) film, respectively.

( $\approx 20$ ).<sup>21–24</sup> The diffraction patterns (DP) and HRTEM images of the annealed Al:HfO<sub>2</sub> films were examined to confirm the crystalline structure, as shown in Figure 11. Although the increased permittivity of the annealed Al:HfO<sub>2</sub> films with a large thickness ( $\geq 10$  nm) was reported,<sup>20</sup> there are no results reported for ultrathin Al:HfO<sub>2</sub> films,  $\leq 5$  nm in thickness. There is no guarantee that thinner films would show the same crystallization as thicker films. Therefore, a rather thick Al:HfO<sub>2</sub> (HAO2) film, ~12 nm in thickness, and an ~3 nm thick Al:HfO<sub>2</sub> (HAO2) film were examined. Images a and b in Figure 11 show the selected area DP (SADP) and cross-sectional HRTEM image of the ~12 nm-thick HAO2 film, respectively. The zone axis was identified as tetragonal HfO<sub>2</sub> corresponding to  $[10\bar{1}]$  in Figure 11a.<sup>21</sup> The tetragonal HfO<sub>2</sub> with the zone axis of  $[0\bar{1}\bar{1}]$  and  $[\bar{1}11]$  was also observed in the ~12 nm thick Al:HfO<sub>2</sub> film, as shown in panels c and d in Figure 11, which was confirmed by the fast Fourier transform (FFT) images in the insets of panels c and d in Figure 11. On the other hand, the ~12 nm thick HAO2 film also contained a proportion of monoclinic structure (data not shown). Therefore, the ~12 nm thick HAO2 film has a tetragonal and monoclinic structure, which is consistent with previous reports.<sup>14–20</sup>

However, the results from the ~3 nm thick HAO2 film were quite different. Images e and f in Figure 11 show the plan-view DP and cross-sectional HRTEM image of an ~3 nm thick HAO2 film, respectively. In SADP, the matrix spots are from the Si substrate with a zone axis of  $[100]$ . There is a ring pattern and spots with a strong intensity indicated by the white arrows. This originated

(50) Lysaght, P. S.; Woicik, J. C.; Sahiner, M. A.; Lee, B.-H.; Jammy, R. *Appl. Phys. Lett.* **2007**, *91*, 122910.



**Figure 12.** (a, b) Si 2*p* core level XP spectra for the control HfO<sub>2</sub> and Al:HfO<sub>2</sub> (HAO2) film before and after PDA, respectively, (c, d) HRTEM image of the control HfO<sub>2</sub> film and Al:HfO<sub>2</sub> (HAO2) film after PDA, respectively.

from the lattice-space of 0.31 nm, which corresponds to the ( $\bar{1}11$ ) plane of a monoclinic HfO<sub>2</sub>.<sup>50</sup> A 0.31 nm lattice fringe was also observed in the HRTEM image of the ~3 nm-thick HAO2 film, as shown in Figure 11f. As the plan-view SADP covers a large area (40  $\mu$ m in diameter), this strongly suggests that most of the ~3 nm thick HfO<sub>2</sub> film remained in the monoclinic structure even after Al doping. This might be because the ultrathin HAO2 film is influenced mainly by the Si substrate, such as Si diffusion into the film and the stress field from the Si substrate. Hence, the superior electrical properties of the ultrathin HAO2 films after PDA cannot be explained by the increased permittivity of the films.

Therefore, the suppressed increases in the EOT of Al:HfO<sub>2</sub> films after PDA must be due to the other reasons mentioned above, suppressed silicate reaction and IL growth. Panels a and b in Figure 12 show Si 2*p* core level XP spectra of the control HfO<sub>2</sub> and HAO2 films before and after PDA, respectively. Although the intensity of the peaks corresponding to Si–O bonding (near the binding energy of 102–104 eV) were similar in both cases of the control HfO<sub>2</sub> and HAO2 film before PDA (Figure 12a),

the increase in the peak intensity after PDA was suppressed in the case of the HAO2 film. This suggests that the Al<sub>2</sub>O<sub>3</sub> in the film suppressed the silicate reaction and IL growth.<sup>51</sup> Hf-aluminate suppresses Hf-silicate formation. Images c and d in Figure 12 show HRTEM images of the control HfO<sub>2</sub> and HAO2 film with 30 ALD cycles after PDA, respectively. The IL thickness of the control HfO<sub>2</sub> and HAO2 film after PDA was ~2.2 and ~2.0 nm, respectively. IL growth during PDA was significantly suppressed in case of the HAO2 film (~0.5 vs ~0.8 nm) because the IL thickness of the control HfO<sub>2</sub> and Al:HfO<sub>2</sub> films before PDA were ~1.4 and ~1.5 nm, respectively. Therefore, the silicate reaction and IL growth during PDA could be suppressed even by a small quantity of Al doping in the film. This can explain the improved thermal stability of the Al:HfO<sub>2</sub> films.

### Conclusions

This study examined the effects of Al doping in HfO<sub>2</sub> thin films (~3–12 nm) on their electrical, structural, and chemical properties. An appropriate Al concentration of ~11% in the HfO<sub>2</sub> film significantly improved the electrical properties. The leakage current density of the Al:HfO<sub>2</sub> film with the optimized Al concentration was reduced by ~2 orders of magnitude compared to that of the control HfO<sub>2</sub> film, even at a given EOT of ~1 nm. The permittivity of HfO<sub>2</sub> film in the thickness range near ~3 nm was not increased by Al-doping, suggesting that the crystalline structure of the film had not transformed to a tetragonal or cubic structure. This is in contrast to thicker films. Al doping largely decreased the oxygen vacancy and C impurity concentrations, which increased the energy gap of the film. This is despite the fact that Al doping itself had little influence on the band gap. The reduced vacancy and impurity concentration also removes the shallow traps. These effects, increased band gap and removal of shallow traps, decreased the leakage current both before and after PDA. The thermal stability of the HfO<sub>2</sub> films was also improved by Al doping because Si diffusion into the film and the oxidation of Si at the interface during annealing were suppressed significantly.

**Acknowledgment.** This study was supported by the System IC 2010 program of the Korean government, the National Research Foundation of Korea (NRF) funded by the Ministry of Education, Science and Technology (2009-0081961), and World Class University program through the Korea Science and Engineering Foundation funded by the Ministry of Education, Science and Technology (R31-2008-000-10075-0)

(51) Yu, H. Y.; Wu, N.; Li, M. F.; Zhu, C.; Cho, B. J.; Kwong, D.-L.; Tung, C. H.; Pan, J. S.; Chai, J. W.; Wang, W. D.; Chi, D. Z.; Ang, C. H.; Zheng, J. Z.; Ramanathan, S. *Appl. Phys. Lett.* **2002**, *81*, 3618.